# Supplementary Information:

# Modulating motility of intracellular vesicles in cortical neurons with nanomagnetic forces on-chip

Anja Kunze[1, 4*], Coleman Tylor Murray[1], Chanya Godzich[1], Jonathan Lin[1], Keegan Owsley[1], Andy Tay[1] and Dino Di Carlo[1, 2, 3*]

*Corresponding authors: anja.kunze@montana.edu, dicarlo@seas.ucla.edu

[1]Department of Bioengineering, University of California, Los Angeles, California 90095, United States

[2]California NanoSystems Institute, University of California, Los Angeles, California 90095, United States

[3]Jonsson Comprehensive Cancer Research Center, University of California, Los Angeles, California 90095, United States

[4]Department of Electrical and Computer Engineering, Montana State University, Bozeman, Montana 59717, United States

This document contains further details about materials and methods and additional images supporting our main article.

**Magnetic forces and chip design**

Local force induction on intracellular vesicle transport was activated through local magnetic field gradients ($\nabla H$) on super paramagnetic nanoparticles (iron oxide core) based on eq. 1, where the resulting magnetic force ($F_{mag}$) depends on the cluster sum ($\sum$) of nanoparticle volume ($V_{p,i}$), and its saturation magnetization ($M_{p,i,sat}$) and the magnetic permeability ($\mu_0$).

$$F_{mag}\,(x,y,z) = \mu_0 \sum_{i=1}^{n} V_{p,i}\; M_{p,i,sat}\; \nabla H(x,y,z) \qquad \text{eq. 1}$$

Local magnetic field gradients were generated through ferromagnetic iron nickel alloys called magnetic elements (MEs). The force range for different cluster sized fMNPs has been characterized previously[1] using Stoke's and Faxen's law and were re-confirmed here through COMSOL simulation. Briefly, 4 µm x 8 µm x 4 µm (H x L x T) MEs generated a magnetic field gradient of ~ 20 A/m$^2$ within a permanent magnetic field ($B_{max}$ = 150 mT, $d_z$ = 1.5 mm, ½ in. × ½ in. × ½ in., Apex Magnets). Correlation between magnetic element size and particle volume dependent magnetic forces was previously estimated[1]. Nanoparticle clusters of r = 400 nm, 490 nm and 750nm resulted in $F_{max,\ x=1\ \mu m}$ = 6.1 – 19.2 pN, 11.3 – 35.3 pN and 40.1 – 125.7 pN,

respectively. The resulting magnetic force stimulation area on chip consisted of an array of six MEs (2 x 3, 4 µm x 8 µm), 16 µm spaced in x-direction and 4 µm spaced in y-direction; or of three MEs in one column 16 µm spaced. The cell adhesion pattern was in symmetry above the ME array covering a surface of 20 µm x 20 µm. A pattern line (7.5 µm wide and 50 µm – 100 µm long) connected the ME cell pattern region with an empty cell region.

**Neuromagnetic chip fabrication**

Fabrication of the neuromagnetic chip is based on previous protocols [2, 3] and was adapted here for advanced cleanroom fabrication processing. Fused silica 10 mm diameter wafers (University Wafer) were cleaned in piranha solution (4:1) for 30 min, washed with DI water and subsequently acetone, methanol and isopropanol, before finally being subjected to oxygen plasma cleaning in a barrel asher (air, 100 $^0$C, 200 W, 2 min). A 50-nm-Ti, 200-nm-Cu and 50-nm-Ti seed layer was then evaporated onto the substrate. SPR 220 photoresist was spun and processed according to specification to form the electroplating mold for nickel-iron alloy. Titanium was etched in 1% HF, and NiFe (80:20) was electroplated in a custom plating setup with a goal of current density of 3 mA cm$^{-2}$ to obtain a thickness of approximately 4 µm. Photoresist was stripped in AZ 300T, and the seed layer was etched in copper etchant (5% acetic acid, 15% H2O2) and titanium etchant (1% HF). The metal layer was then passivated by deposition of 100 nm PECVD SiN. A planarizing layer of 1002F photoresist1 was spun with an acceleration of 500 r.p.m./s, 200 r.p.m for obtaining a desired substrate thickness of approximately 5 µm. The substrate was prebaked for 15 min at 65 °C then 15 min at 95 °C, followed by UV flood exposure of ~1020 mJ and ending with a post exposure bake of 1 min at 65 °C and 2 min at 95 °C. A second lithography layer was performed on top of the planarizing 1002F[4] layer to produce openings for cell adhesion patterns using SPR 220-3 with the same exposure and development conditions listed before.

Chips were stored at room-temperature shielded from light until further usage. Prior neuronal cell seeding, opened 1002F structures were $O_2$ plasma activated (38 W, 45 s, 500 mTorr) and SPR 220-3 was removed through a 100% acetone rinse. A polymeric 0.05 % (w/v) Pluronics, 25 % (v/v) PLL in PBS solution was subsequently co-adsorbed to oxygen plasma activated surface, after 20 min UV sterilization for 16 h at 37 $^0$C. Prior cell seeding, polymeric solution was aspirated, chips were washed with sterile water and culture medium (Neurobasal, 10% horse serum) added.

**Numerical modeling of magnetic forces**

To model the magnetic force system (Fig. S1a), three simulations were created in COMSOL Multiphysics 4.4. First, a millimeter-scale simulation of a neodymium magnet was used to study the magnetic field characteristics in the vicinity of a permanent magnet. This bulk field was used as a boundary condition for the micro-scale simulations (Fig. S1b). Permalloy MEs were assumed to have relative magnetic permeability (against air) of 6500. Magnetic particles were assumed to have magnetic susceptibility of 0.045. We consider only magnetic forces within a plane located 1 µm from the surface of the microelements. In general, the force $F_{mag,p}$ on a single particle with volume ($V_p$) due to a magnetic field $B$ is given by eq. 2[5]:

$$\overrightarrow{F_{mag,p}} = \rho V_p \nabla\left(\overrightarrow{M_0} \cdot \vec{B}\right) + \frac{V_p \chi_p}{\mu_0}\left(\vec{B} \cdot \nabla\right)\vec{B} \quad \text{eq. 2}$$

With ρ and $\chi_p$ as density and magnetic susceptibility of the particle, respectively. For a particle with no initial magnetization $\vec{M}_0$, the first term vanishes and magnetic forces are computed entirely by induced magnetization due to the bulk field, in the direction of the magnetic field gradient. These computations were performed in python and streamplots created by the matplotlib module (Fig. S1c and d).

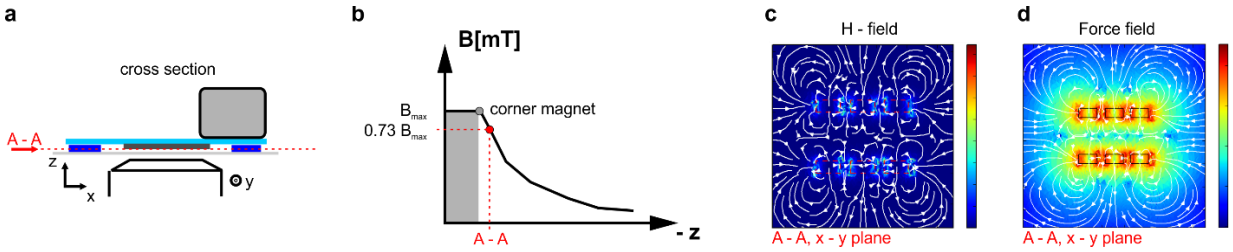


Figure S1: Experimental setup and boundary conditions for magnetic field simulation. (a) Schematic illustrates the inverted chip above an objective and the position of the 150 mT permanent magnet. (b) Magnetic field decay away from the permanent magnet yields ~ 110 mT in the x-y plane of the magnetic elements. (c) 6 ME pattern and its magnetic field deformation plot (H-field) with (B-stream lines). (d) Resulting magnetic force gradient projected to x-y plane.

The resulting magnetic forces have an x- and y- component. Depending on the position and directionality of molecular motor driven flow, forces can lead to hindered, accelerated or reoriented motion (Fig. S2).

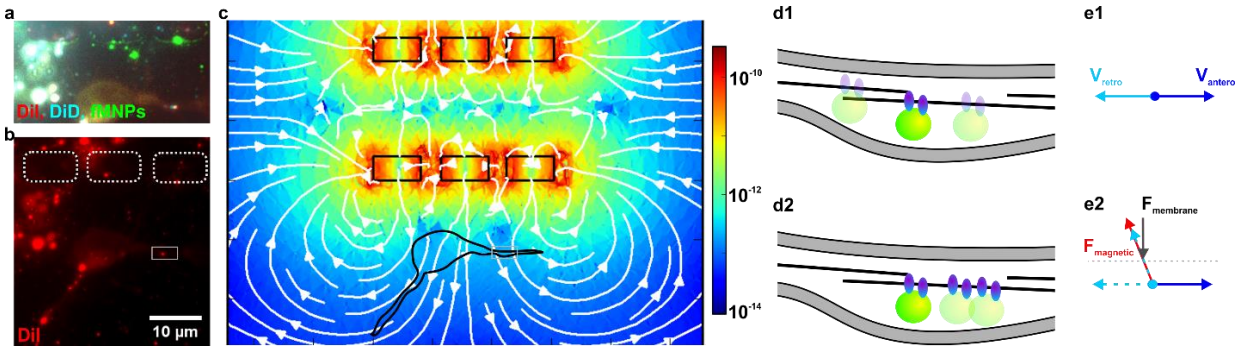


Figure S2: Functionalized magnetic nanoparticles can alter the moving direction of vesicle in neurons. (a) Fluorescent image shows a neuron with co-localization signal spots of fMNPs and vesicles (DiD, DiI). (b) Fluorescent image of DiI vesicle spots near the six 4 µm x 8 µm ME structures (dotted rectangles). (c) Heat-map surface plot of COMSOL – Matlab modelled magnetic force distribution at the six ME structure. (d1) Vesicle transport along microtubules in neurons driven by kinesin (anterograde) and dynein motors (retrograde). (d2) Magnetic force applying a stall force to the transport motors restricting retrograde and anterograde transport. (e1) Schematic shows vesicle transport directions without magnetic forces. (e1) Retrograde vesicle transport direction gets blocked.

## Rat neuronal cell culture

Following neuronal cell culture protocol from Kunze *et al.*[1], rat cortical hemispheres were dissected from whole embryonic rat brains (E18, BrainBits) and dissociated with 10 % (v/v) Papain (Carica papaya, Roche) in Hibernate®-E (BrainBits) at 35 $^0$C for 15 min. After dissociation,

cortical neurons were centrifuged (6 min, 600 rpm, at room temperature) and seeded at a cell concentration of $2x10^6$ cells/ml. For seeding, 150 - 300 µl cell suspension was drop wise added to the chip surface. Loose cells were removed after 2 h incubation through a gentle washing step and incubated overnight (95 % air, 5 % $CO_2$, 37 $^0$C) in Neurobasal serum free with 2 % (v/v) serum free B-27®, 1% (v/v) GlutaMAX™ and 1% (v/v) Pen Strep.

### Human neuronal cell culture

Pre-differentiated, mixed population neurons derived from human induced pluripotent stem cells (human iPSC line, XCL-1) were thawed drop-wise in 37°C neuronal medium (Neuro Kit, XN-001-S-NH, Xcell Science) and counted on a hemocytometer following resuspension. Cells were then seeded at $2x10^6$ cells/ml density by placing 250 µl on chip and cultured in complete neuronal medium for the remainder of the study.

Exposing human neuronal cells to magnetic fields resulted in no significant changes in motion classification in contrast to rat cortical neurons (Fig. S3)

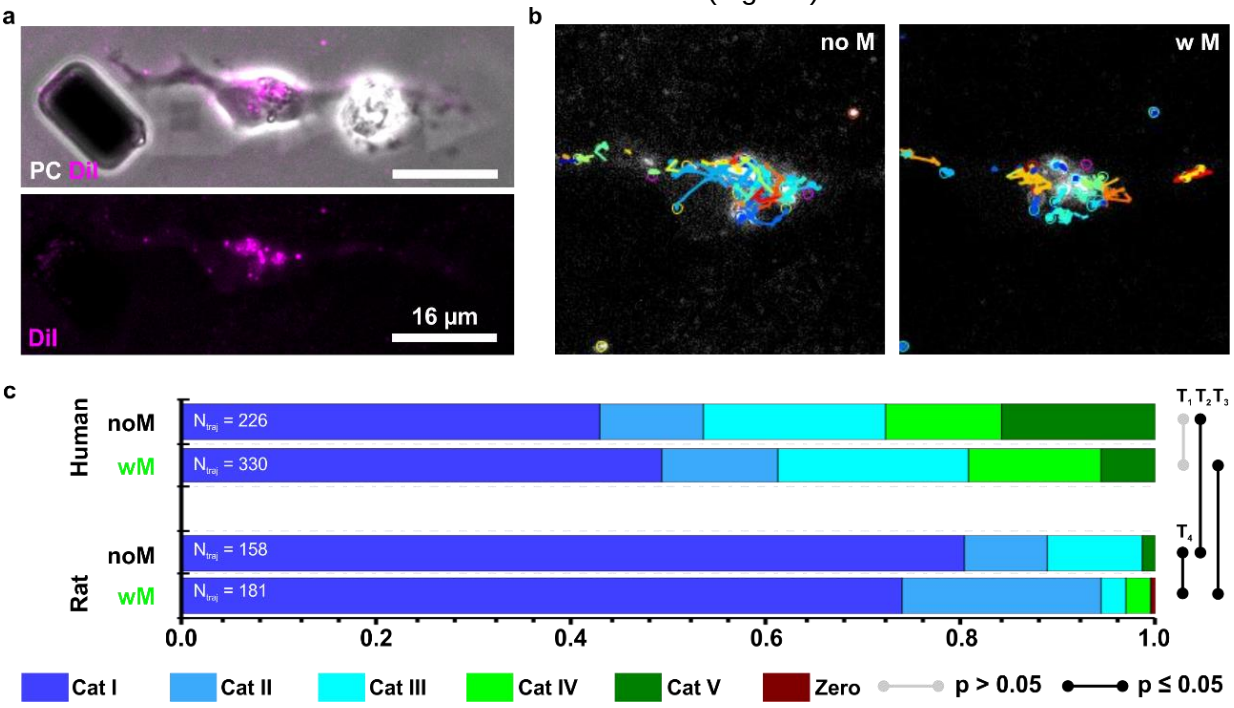


Figure S3: The cellular origin plays a role in sensing magnetic fields. (a) Representative phase contrast image of a human stem-cell derived excitatory neuron (2 days *in vitro*) above PLL pattern adjacent to a ME without fMNPs stained with DiI for lipid vesicles. (b) Vesicle trajectories without (no M) and with (w M) magnetic field exposure. (c) Bar histogram plot (H) of relative counts per category for DiI vesicle tracks with in human versus rat neurons with (wM) and without (noM) magnetic field. $N_{traj}$ = total number of trajectories. Line-connectors demonstrate statistical test result (p-value) for Chi-Square test with $h_0$: $H_{Human,noM} = H_{Human,wM}$, or $H_{Human,noM} = H_{Rat,wM}$

### Cell staining and fluorescent labeled vesicle trafficking

To visualize different vesicle types in rat cortical neurons we used CellLight® Late Endosomes-RFP, BacMam 2.0 to fluorescently label Rab7a proteins in late endosomes, Vybrant® DiI (1,1'-dioctadecyl-3,3,3',3'- tetramethylindodicarbocyanine 4-chlorobenzenesulfonate salt) and DiD (1,1'-dioctadecyl-3,3,3',3'-tetramethylindocarbocyanine perchlorate) Cell-Labeling Solution to

highlight lipid vesicles and LysoTracker® Deep Red to stain acidic lysosomes. RFP late endosomal transfection was combined with DiD (Far-red fluorescent) vesicle staining or Deep Red LysoTracker staining and with DiI (red-fluorescent) with DiD or LysoTracker. Baculovirus transfection of Rab7a was started 16 h prior to nanoparticle exposure in neurons at day one in culture with 50 particle per cell. LysoTracker labeling was optimal when loaded 2 h prior to imaging at a final concentration of 100nM in 5 ml. DiD and DiI staining was achieved following vendor protocol. Briefly, 100 µl of a 0.5% (v/v) DiI or DiD/media solution was administered to neurons on chip and incubated up to 1 h.

Co-staining of DiI with DiD in cortical neurons highlight two different sub-populations of vesicles (Fig. S4). We found almost all late endosomal (B-LE) staining overlapping with DiD stains and some lysosomal (Lyso) staining overlapping with DiI stainings.

Nanoparticle cluster may impact vesicle size. To test this assumption vesicle size was estimated based on 2D area measure (particle size measure). The histogram plot in Fig. S4b shows DiI stained vesicle size distribution for five binned area sizes below A < 0.6 µm$^2$ (d < 0.87 µm). Note the averaged diameter of Chi-NP clusters was around 630 nm. DiI vesicles seem not to change their size distribution under Chi-NP exposure. In contrast, DiD vesicle size distribution showed an increase number of small vesicles (d < 0.36 µm), which may be linked to Chi-NP exposure, however do not contain detectable fluorescent Chi-NPs. It is always possible that DiD vesicle contain large portions of smaller Chi-NPs, however, the magnetic force acting on these smaller particles will be below the pico-newton range and seemed not to have an effect on the DiD vesicle motion in our experiments.

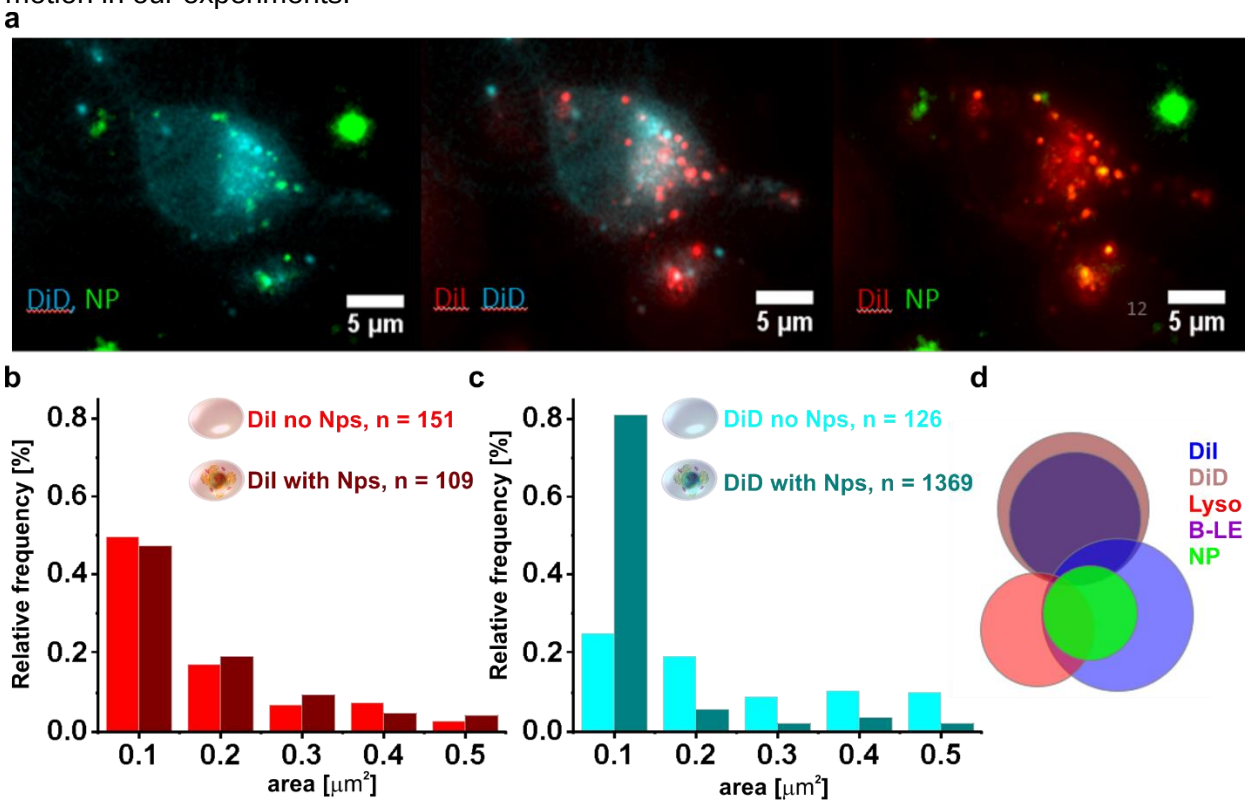


Figure S4: Cortical neuron with uptaken nanoparticles and lipid membrane stainings. (a) Fluorescent images of DiD (cyan) and DiI (red) stained cortical neurons containing Chi-NP (green). (b), (c) Normalized histogram plots of (b) DiI and (c) DiD stained vesicle size distribution in neurons after incubation with Chi-NPs and without particles as a control. (d) Venn diagram represent the similarities between the observed vesicle stains and the fluorescent intracellular nanoparticles in cortical neurons (DiI & DiD: vesicle stains, Lyso: lysosomes, B-LE: late endosomes. NP: nanoparticles).

## Analyzing vesicle movement

Multi-channel stacks were further processed as 8-bit color image sequence, corrected for transformative shift with StackReg plugin (ImageJ) in case of occurance and histogram corrected for autobleaching. Subsequent, moving vesicle dots were tracked using TrackMate[6] (DOG detector[7], 0.8 µm blob diameter; filters: median intensity, estimated diameter and signal/noise ratio; linking: 1.6 µm) and exported into .xml files. A MATLAB script excludes tracks shorter than 108 s, generates star plots for tracks ($\Delta t_{max}$ = 2 min), computes mean square displacement (MSD, Δt = 57 s, $\tau = 3\,s$, eq. 3[8]), averaged "caging" diameter (CD, Δt = 114 s, eq. 4[9]), total traveled length (L, Δt = 114 s, eq. 5) and averaged velocity (all tracks, eq. 6) and outputs frequency for categorized vesicle behavior based on CD and L.

$$MSD = \frac{1}{N-\tau}\sum_{\tau=1}^{N-\tau}\left|\binom{x_{i+1}}{y_{i+1}} - \binom{x_i}{y_i}\right|^2 \qquad \text{eq. 3}$$

$$CD_{avg} = \frac{1}{k}\sum_{i=1}^{k=\frac{t_{max}}{\tau}} CD_i(t_i) \qquad \text{eq. 4}$$

$$L_{total} = \sum_{i=1}^{k} L_i \qquad \text{eq. 5}$$

$$V_{avg} = \frac{1}{k}\sum_{i=1}^{k}\frac{L_i}{t_i - t_{i-1}} \qquad \text{eq. 6}$$

MSD of vesicle tacks were then compared with MSD model[8] (2D case) of stationary processes for free diffusion (eq. 7), intracellular free diffusion (eq. 8) and confined diffusion (eq. 9).

$$MSD_{diff} = 4D\tau \qquad \text{eq. 7}$$

$$MSD_{cell} = 4\,k_{cell}\,D_{H_2O}\tau \qquad \text{eq. 8}$$

$$MSD_{conf} = R_c^2\left(1 - e^{-4k_{cell}D_{H_2O}\tau/R_c^2}\right) \qquad \text{eq. 9}$$

## Vesicle size effect on diffusive motion pattern

Vesicle dynamics are analyzed based on Mean-Square-Displacement (MSD), which are calculated for each individual vesicle trajectory. Besides MSD vesicle dynamics can also be characterized based on a caged motion pattern, which allows to compute a caging diameter. The MSD is then plotted over its time-lag and indicates diffusive versus confined, or directed motion. Diffusive motion can be further differentiated into Brownian (linear correlation), super-, or sub-diffusive (power law correlation) motion. In cortical neurons DiD vesicles were found to show on average a diffusive motion pattern (Fig. S5a). In contrast, DiI labeled vesicles move slightly faster than Brownian motion even without fMNPs (Fig. S5b). After 6h exposure to Chi-NPs, which led into nanoparticle uptake into neurons, DiI vesicles, which also fluorescently co-localize with fluorescent signal from Chi-NPs, show on average super-diffusive and directed motion pattern (Fig. S5c).

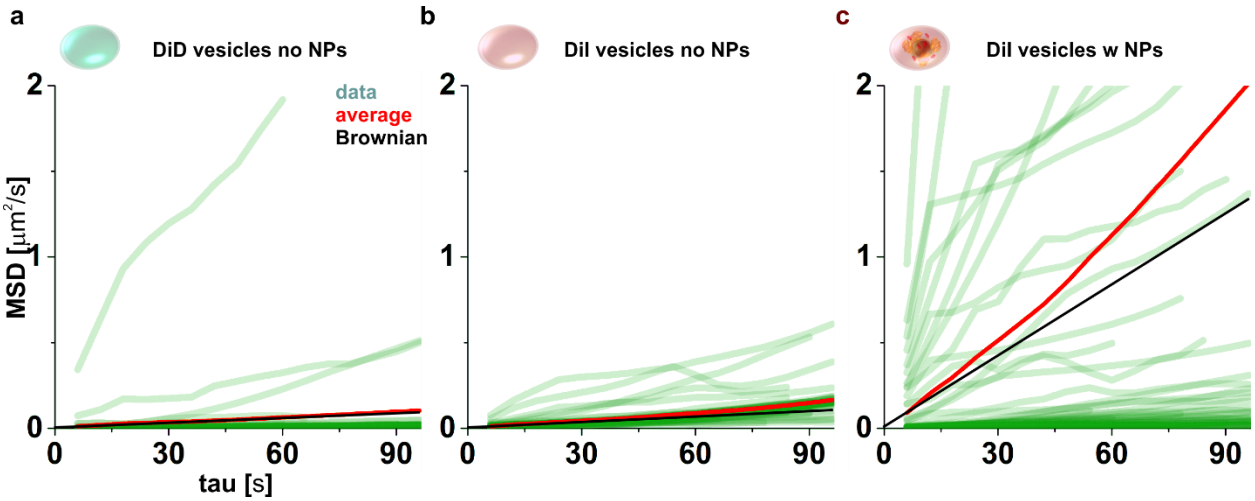


Figure S5: MSD plots for DiD and DiI labeled vesicles in cortical neurons (2d old). (a) DiD and (b) DiI vesicles without exposure to nanoparticles and therefor containing no fMNPs. (c) MSD of DiI vesicles that were exposed Chi-fMNPs.

## Altering vesicle trafficking through magnetic force induction

To induce an intracellular mechanical force, cortical neurons were introduced to 30 µg/ml chitosan or dextrax coated green fluorescent iron oxide nanoparticles (superparamagnetic, $h_{d,vendor}$ = 100 nm, nano-screenMAG/G-Chitosan or -D, Chemicell) for 6 h prior to experimental manipulation. Residual medium containing unabsorbed nanoparticles was removed and neurons washed with pre-warmed media. Neuromagnet chips were then transferred to the imaging platform and immersed into $CO_2$-independent pre-warmed Hibernate E Low Fluorescence imaging media (BrainBits).

Prior magnetic force induction vesicle motion was monitored and individual cell position saved for further experimental procedures. We placed a neodym magnet $B_{max}$ = 150 mT (½ inch x ½ inch x ½ inch, Apex Magnets) on top of the chip slightly shifted towards the right side to allow phase contrast microscopy and started monitoring vesicle movement with a delay of 1 – 2 min after magnetic field and force induction. For resulting magnetic field and magnetic gradient near the magnetic elements see figure S1. To obtain high resolution images with a small working distance objective (60x oil, NA: 1.42, WD: 380 µm), we fabricated PDMS gaskets (10:1, ~ 500 µm thick) to immerse the chip inverted into neuronal medium (Fig. S6) in a glass bottom dish (In Vitro Scientific).

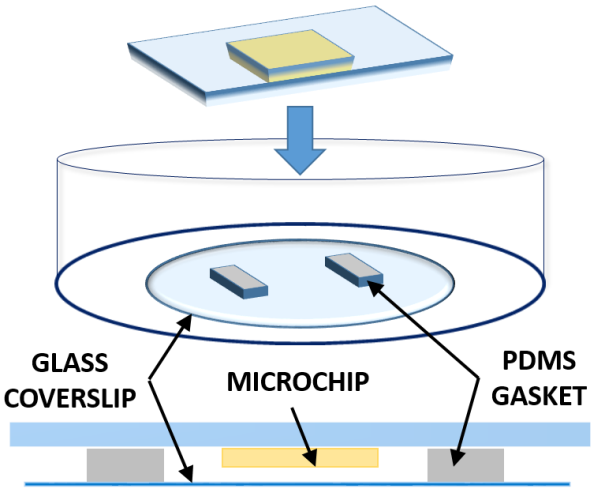


Figure S6: Schematic drawing of glass bottom dish with PDMS gaskets that were fabricated at a height of 550 – 650 µm to place neurons on top of the microchip inverted into a medium containing dish. Neurons are located at a final distance of ~ 50 µm above the imaging cover slip.

## Nanoparticle size and charge characterization

Nanoparticle cluster sizes and medium dependent ζ-potentials were evaluated by Zetasizer Nano-ZS (Malvern Instruments, Ltd.) using dynamic light scattering through disposable folded capillary cells. Chitosan or dextran coated fluorescent nanoparticles (Chemicell, 1.2 µl/ml each) were added to sterile Nanopure™ water (8.2 MΩ cm) and Neurobasal™ medium (B27, glutamate, Pen Strep) and pre-warmed to 37°C. Nanoparticle suspensions were vortexed for 20 s before loading into the capillary cells.

Three rounds of measurements were averaged for both ζ-potentials and cluster size measurement. Hydrodynamic cluster sizes were discerned from 10 nm peak observed in medium due to the presence of proteins[10].

As a reference, hydrodynamic radius was determined of non-functionalized iron oxide nanoparticles ($h_{vendor}$ = 100 nm, Chemicell) in PBS, water and neurobasal media. The resulting values are 163 ± 8 nm, 161 ± 11 nm and 178 ± 13 nm, respectively. The difference in size between the vendor and the measured hydrodynamic radius raised questions regarding the accuracy of the Zetasizer measurements. We took transmission electron microscopy images (TEM) of the Chemicell nanoparticles. Figure S7 shows the black core of iron oxide from TEM imaging. Analyzing the diameter of the iron core results in an average value of 103 ± 21 nm. The whole nanoparticle cluster measures ~ 500 nm in diameter. The uptake of different fMNP cluster sizes has been extensively characterized in Kunze et al.[1]

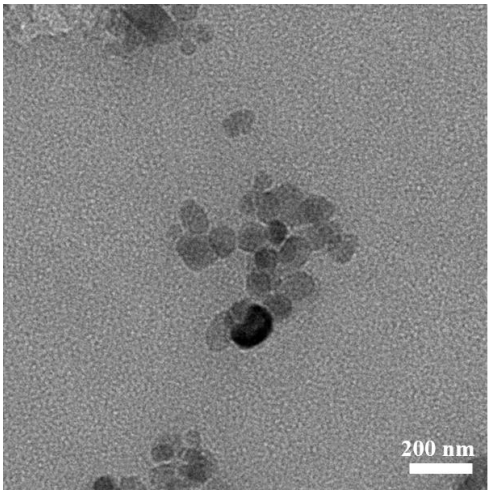

Figure S7: TEM image shows iron oxide core content of superparamagnetic nanoparticles used for our study.

## Blocked and accelerated vesicle trafficking

Altering vesicle transport behavior was achieved through blocking and activating kinesin-5 motors using monastrol and insulin, respectively. For blocking, we prepared 1 mM monastrol (Sigma, M8515) stock solution by dissolving lypophylized powder (≥98%, HPLC) in DMSO. An aliquot of 100 µl was dissolved in 1 ml Hibernate E and chips were immersed into imaging solution and let incubated for 10 min prior to imaging. Kinesin transport was accelerated through the addition of 10% (v/v) human insulin (Sigma, I9278, 10mg/ml stock), to media in the imaging platform, where neurons were incubated for at least 20 min prior imaging. Note: Insulin concentration was intentionally chosen high above physiological condition to trigger a cells response within few minutes.

## Image acquisition

Fluorescently stained cortical neurons were semi-automated captured using a programmable stage (MIV-2000 Te/Ti 2000 He, ASIimaging) on a Nikon microscope (Eclipse Ti, DAPI, FITC, TRICT, CY-5 filters, 60x air, NA = 0.85, and 60x oil, NA = 1.4 objectives) with a CCD camera (QuantEM:512SC EM, Photometrics) operated at fixed gain. Cell position was captured and referenced with magnets applied in positive-X-axis pointing towards right. Channel exposure times were set to CY-5: 800 ms, TRITC: 800 ms and FITC: 500 ms. Multi-channel image acquisition was programmed with 3 s – 6 s time intervals to capture 3 channels/time point. Multi-stacked TIFF based (16-bit) imaging files were further processed using ImageJ and FIJI.

## Statistical evaluation

Velocity and length distributions were tested against normal distribution. Appropriate ANOVAs were chosen based on parametric and non parameteric test routines (OriginPro 9, $p<0.001$ or otherwise indicated). Histogram distribution of CD-L categories were compared using Chi-Square test[11] and were visualized based on $p > 0.05$ (not significant) and $p \leq 0.05$ (significant different). Vesicle measurements were paired, if not otherwise indicated. We accounted for cell position and cell morphology and exclude star-shaped cell morphology (Fig. S8)

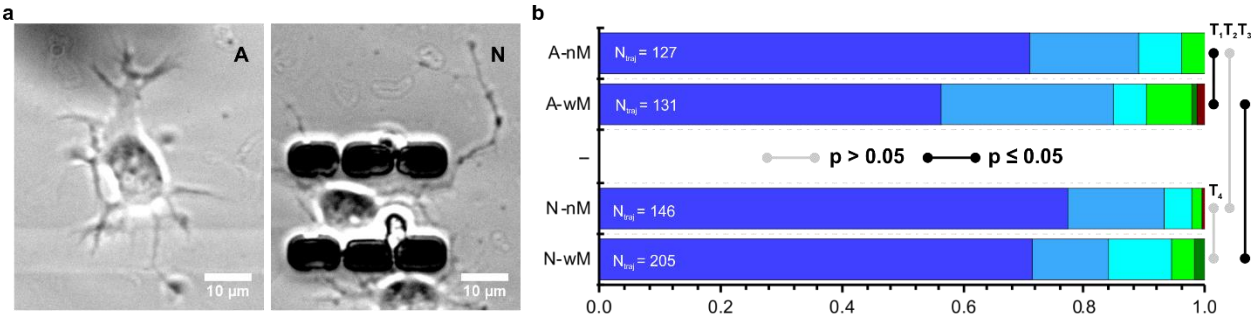


Figure S8: Supplemental image for figure 5 and 6. The magnetic field effect is highly sensitive to cell location and morphology even without magnetic nanoparticles. (a) Representative phase contrast image of brain cells from the rat cerebral cortex (A) next and (N) above 6 ME pattern. Also cell in A has a slight different morphology than cell in N, adhering to PLL pattern in N but not in A. (b) Bar histogram plot of relative counts per category for DiI vesicle tracks for cell A and cell N. $N_{traj}$ = total number of trajectories. Line-connectors demonstrate statistical test result (p-value) for Chi-Square test with $h_0$: $H_A = H_N$.

## Demonstration of nanoparticle transport in DiI labeled vesicles

Comparing the position of Chi-NPs with the position of DiI labeled vesicles shows coherent movement pattern for both nanoparticles and vesicles, see white circle in Figure S9. Note that red images are captured ~ 300 ms later than green images. Figure S9 also shows that not all nanoparticles associate with lipophilic dye stained intracellular vesicles, highlighted by the arrow A. Another challenge for nanoparticle tracking is the low emitted fluorescent signal, which might be hidden and thus cannot be detected.

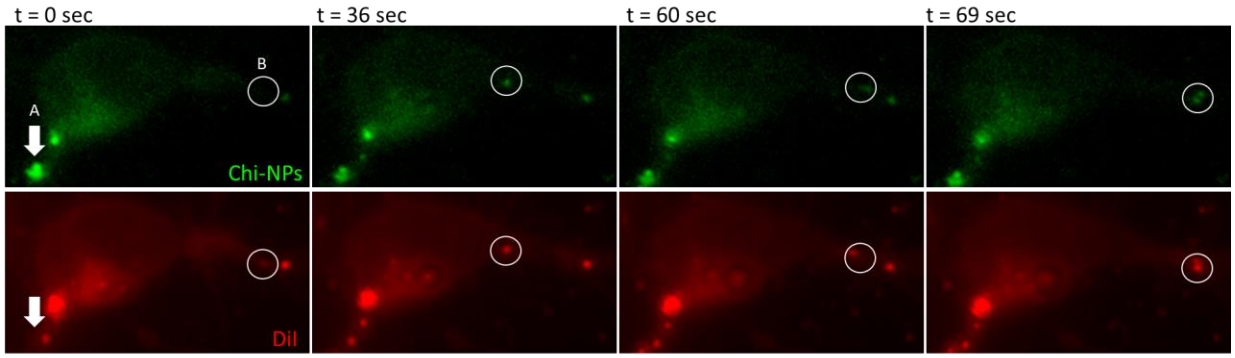


Figure S9: Fluorescent images extracted from video files show nanoparticle transport in relation to vesicle transport.

## Videos

Video V1: V1-RatNeuron_DiI_ChiwNP-nM: Video shows DiI vesicle motion in rat cortical neurons containing Chi-NPs (no magnetic field). Scale bar = 5 µm.

Video V2: V2-RatNeuron_DiI_ChiwNP-wM: Video shows corresponding neuron from video V1 now under magnetic field exposure. Scale bar = 5 µm.

Video V3: V3-RatNeuron_DiI_noNP-nM: Video demonstrates DiI vesicle motion without any nanoparticles.

Video V4: V4-RatNeuron_Activ_DiI_ChiNP-nM: Video represents activated vesicle motion (DiI staining) under insulin enriched media with chitosan coated nanoparticles (Chi-NP) and no magnetic field.

Video V5: V5-RatNeuron_Block_DiI_ChiNP-nM: Video represents blocked vesicle motion (DiI staining) by monastrol enriched media with chitosan coated nanoparticles (Chi-NP) and no magnetic field.

Video V6: V6-HumanNeuron-NoNP-noM : Video shows single human neuronal cell derived from iPS with stained vesicle motion (no magnetic field, no nanoparticles).

Video V7: V7-HumanNeuron-NoNP-wM: Video shows corresponding single human neuronal cell from video V6 with magnetic field exposure. (no nanoparticles).

**Literature**


1. A. Kunze, P. Tseng, C. Godzich, C. Murray, A. Caputo, F. E. Schweizer and D. Di Carlo, *ACS Nano*, 2015, **9**, 3664-3676.
2. P. Tseng, J. W. Judy and D. Di Carlo, *Nat Meth*, 2012, **9**, 1113-1119.
3. P. Tseng, D. Di Carlo and J. W. Judy, *Nano Letters*, 2009, **9**, 3053-3059.
4. J.-H. Pai, Y. Wang, G. T. A. Salazar, C. E. Sims, M. Bachman, G. P. Li and N. L. Allbritton, *Analytical Chemistry*, 2007, **79**, 8774-8780.
5. S. S. Shevkoplyas, A. C. Siegel, R. M. Westervelt, M. G. Prentiss and G. M. Whitesides, *Lab on a Chip*, 2007, **7**, 1294-1302.
6. N. Perry, J.-Y. Tinevez and J. Schindelin, TrackMate - Fiji, http://fiji.sc/TrackMate, (accessed 6/4/2015).
7. N. Chenouard, I. Smal, F. de Chaumont, M. Maska, I. F. Sbalzarini, Y. Gong, J. Cardinale, C. Carthel, S. Coraluppi, M. Winter, A. R. Cohen, W. J. Godinez, K. Rohr, Y. Kalaidzidis, L. Liang, J. Duncan, H. Shen, Y. Xu, K. E. G. Magnusson, J. Jalden, H. M. Blau, P. Paul-Gilloteaux, P. Roudot, C. Kervrann, F. Waharte, J.-Y. Tinevez, S. L. Shorte, J. Willemse, K. Celler, G. P. van Wezel, H.-W. Dan, Y.-S. Tsai, C. O. de Solorzano, J.-C. Olivo-Marin and E. Meijering, *Nat Meth*, 2014, **11**, 281-289.
8. N. Monnier, S.-M. Guo, M. Mori, J. He, P. Lénárt and M. Bathe, *Biophysical Journal*, 2012, **103**, 616-626.
9. S. Nofal, U. Becherer, D. Hof, U. Matti and J. Rettig, *The Journal of Neuroscience*, 2007, **27**, 1386-1395.
10. S. S. Yu, C. M. Lau, S. N. Thomas, W. G. Jerome, D. J. Maron, J. H. Dickerson, J. A. Hubbell and T. D. Giorgio, *International Journal of Nanomedicine*, 2012, **7**, 799-813.
11. K. J. Preacher, *Journal*, 2001.